A Novel Method of Reducing Commutation Torque Ripple for Brushless DC Motor Based on Cuk Converter

Wei Chen, *Member, IEEE*, Yapeng Liu, Xinmin Li, Tingna Shi, *Member, IEEE*, and Changliang Xia, *Senior Member, IEEE*

***Abstract*—In this paper, based on Cuk converter, a novel commutation torque ripple reduction strategy is proposed for the brushless DC motor. Output modes (buck–boost mode and boost mode) of the Cuk converter during the commutation period and normal conduction period are altered by designing a mode selection circuit, which can reduce commutation torque ripple over the entire speed range. During the commutation period, Cuk converter operates in the boost mode to step up the input voltage of three-phase bridge inverter and then meet the voltage demand of commutation period, such that the commutation torque ripple can be reduced by keeping the noncommutated current steady. In order to improve the utilization rate of the converter, during the normal conduction period, Cuk converter operates in the buck–boost mode and the input voltage of three-phase bridge inverter is regulated by adopting the pulse amplitude modulation (PAM) method without the inverter pulse width modulation chopping, which can reduce the voltage spike damage to the motor windings caused by turn-on/off of MOSFET in the inverter and simplify the program of modulation method further. The experimental results verify the correctness of the theory and the effectiveness of the proposed approach.**

***Index Terms*—Brushless DC motor (BLDCM), commutation torque ripple reduction, Cuk converter, mode selection circuit.**

I. Introduction

BRUSHLESS DC motor (BLDCM) has received a great deal of attention in many industrial applications, owing to its simple structure, high power density, and high reliability [1]–[3]. However, larger commutation torque ripple may bring about vibration and noise, which restricts its application in high-precision servo systems. Therefore, commutation torque ripple reduction is of great significance to expand applications of BLDCM.

Manuscript received May 18, 2016; revised July 25, 2016; accepted September 12, 2016. Date of publication September 23, 2016; date of current version February 27, 2017. This work was supported in part by the National Key Basic Research Program of China (973 Program) under Grant 2013CB035600, and in part by the National Natural Science Foundation of China under Grant 51577126. Recommended for publication by Associate Editor B. Singh.

W. Chen, Y. Liu, X. Li, and T. Shi are with the School of Electrical Engineering and Automation, Tianjin University, Tianjin 300072, China (e-mail: chen_wei@tju.edu.cn; yapengliu@tju.edu.cn; lixinmin@tju.edu.cn; tnshi@tju.edu.cn).

C. Xia is with the School of Electrical Engineering and Automation, Tianjin University, Tianjin 300072, China and also with Tianjin Engineering Center of Electric Machine System Design and Control, Tianjin 300387, China (e-mail: motor@tju.edu.cn).

Color versions of one or more of the figures in this paper are available online at http://ieeexplore.ieee.org.

Digital Object Identifier 10.1109/TPEL.2016.2613126

An original analytical study on commutation torque ripple is presented in [4], in which it is pointed out that the commutation torque ripple, which reaches 50% of the average torque, can be reduced by keeping the noncommutated phase current steady. Different pulse width modulation (PWM) methods are adopted to keep the noncommutated phase current steady during commutation period in [5]–[12]. In [5]–[9], the motor speed is divided into high speed and low speed, and different two-phase modulation methods during the commutation period are used, respectively, according to different speed ranges. However, when the motor operates near the switching condition of high speed and low speed, the frequent switch of the modulation methods caused by speed fluctuation will appear, which may reduce the stability of the system. Thereby, the three-phase modulation methods in [10], [11] are used during the commutation period to maintain the steady noncommutated phase current over the entire speed range. However, the switch of modulation methods between the normal conduction period and the commutation period is required, which complicates the modulator design. In addition, the same two-phase modulation method during both the normal conduction period and commutation period is used to simplify the modulator design in [12], in which the PWM only applies to the noncommutated phase during commutation period. The commutation torque ripple in low speed range can be reduced by using the PWM method, whereas when the motor works at high speed, especially under rated condition, the PWM method could not effectively reduce the commutation torque ripple due to finite input voltage of the three-phase bridge inverter [8], [13], [14].

In order to reduce the commutation torque ripple in high speed range, a DC–DC converter is introduced to increase the input voltage of the three-phase bridge inverter in [15] and [16]. Z-source inverter is added in [15], and the required input voltage of the inverter is obtained by adjusting the duty cycle of shoot-through vectors to keep noncommutated phase current steady. However, the input voltage of the inverter is larger than the power supply voltage during both the normal conduction period and commutation period. In [16], during the normal conduction period, the BLDCM is supplied by power voltage and the desired voltage for commutation period is adjusted by the SEPIC converter. During commutation period, the SEPIC converter is applied by a switch selection circuit to suppress the commutation torque ripple. However, the converter is employed only in

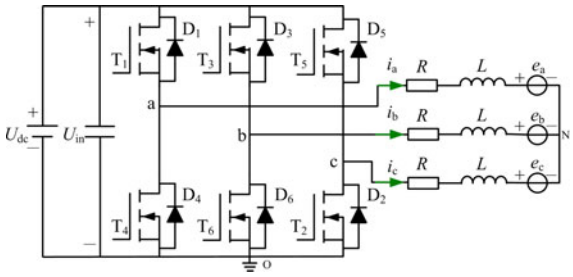

Fig. 1. Equivalent circuit of the BLDCM drive system.

commutation period and the effect of commutation torque ripple suppression depends on dynamic response of the SEPIC converter.

In the field of commutation torque ripple reduction, there are still several challenges for the existing methods. In order to avoid switching modulation methods, the commutation torque ripple reduction strategy should be applied over the entire speed range. In addition, the same modulation method should be adopted during both the normal conduction period and commutation period. In order to effectively reduce the commutation torque ripple in the high speed range, the DC–DC converter is required to step up the input voltage of the three-phase bridge inverter and meet the voltage demand of commutation period; meanwhile, the utilization of the DC–DC converter should be enhanced as far as possible.

Cuk converter as a basic DC–DC converter has advantages of continuous input and output current and low output voltage ripple [17], and it has been used to drive BLDCM [18]. In recent years, the research on Cuk converter mainly concentrates in topological theory, PWM technique and control method [19]–[23]. Cuk converter has three output modes (buck mode, boost mode, and buck–boost mode), and different modes output different voltages with the same operational principle [24], which provides the possibility to step up the input voltage of the three-phase bridge inverter.

In this paper, a mode selection circuit is designed to alter the output mode of the Cuk converter. During commutation period, Cuk converter operates in the boost mode and its output voltage can meet the voltage demand of commutation period, such that the commutation torque ripple can be reduced effectively by keeping the noncommutated phase current steady over the entire speed range. During the normal conduction period, the Cuk converter operates in the buck–boost mode and the input voltage of the three-phase bridge inverter is regulated by the PAM method without the inverter PWM chopping, which can reduce voltage spike damage to the motor windings caused by turn-on/off of MOSFET in the inverter, simplify the program of modulation method and improve the utilization rate of the Cuk converter.

II. Analysis of Commutation Torque Ripple for BLDCM

The equivalent circuit of the BLDCM drive system with the assumption of three-phase symmetric stator windings is shown in Fig. 1. Each phase winding can be equivalent to the resistance, inductance, and back electromotive force (EMF) in series.

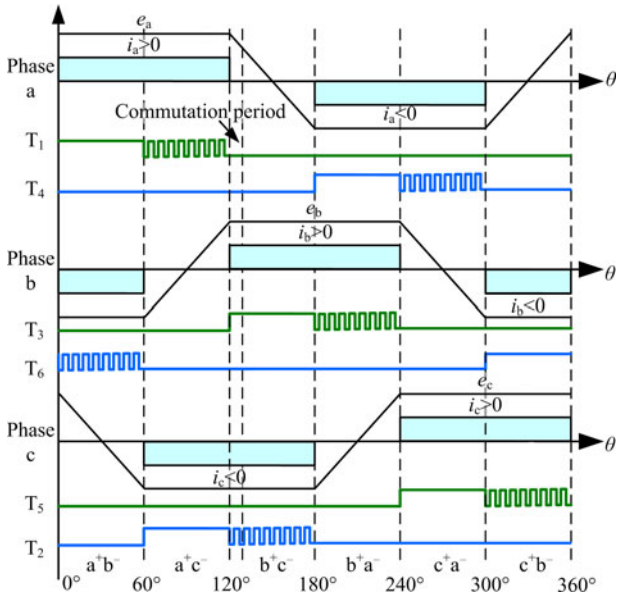

Fig. 2. Ideal back-EMFs and ideal phase currents of BLDCM with ON-PWM modulation method.

The three-phase terminal voltages of BLDCM are expressed as

$$\begin{cases} u_{\mathrm{a}} = Ri_{\mathrm{a}} + L\frac{\mathrm{d}i_{\mathrm{a}}}{\mathrm{d}t} + e_{\mathrm{a}} + u_{\mathrm{No}} \\ u_{\mathrm{b}} = Ri_{\mathrm{b}} + L\frac{\mathrm{d}i_{\mathrm{b}}}{\mathrm{d}t} + e_{\mathrm{b}} + u_{\mathrm{No}} \\ u_{\mathrm{c}} = Ri_{\mathrm{c}} + L\frac{\mathrm{d}i_{\mathrm{c}}}{\mathrm{d}t} + e_{\mathrm{c}} + u_{\mathrm{No}} \end{cases} \tag{1}$$

where u_{a}, u_{b}, and u_{c} are the terminal voltages of the three-phase stator windings, i_{a}, i_{b}, and i_{c} are the phase currents, e_{a}, e_{b}, and e_{c} are the phase back EMFs, R is the phase resistance, L is the phase inductance, and u_{No} is the neutral point voltage of the motor.

The electromagnetic torque T_{e} of BLDCM is given by

$$T_{\mathrm{e}} = \frac{e_{\mathrm{a}}i_{\mathrm{a}} + e_{\mathrm{b}}i_{\mathrm{b}} + e_{\mathrm{c}}i_{\mathrm{c}}}{\omega_{\mathrm{m}}} \tag{2}$$

where ω_{m} is the rotor mechanical angular velocity.

BLDCM normally operates in the two-phase conduction mode with six steps commutation, which means only two windings are energized and the other winding is floating in the normal conduction period. Fig. 2 illustrates the ideal back EMFs and ideal phase currents of BLDCM with ON-PWM modulation method (for example, when phase "a" is a positive phase, MOSFET T_1 in upper-arm of phase "a" is ON in the first 60° electrical angles and chopping in the latter ones).

Take "a^+c^-" as an example, where phase "a" is a positive phase and phase "c" is a negative phase, and then $i_{\mathrm{a}} = -i_{\mathrm{c}}$, $i_{\mathrm{b}} = 0$, $e_{\mathrm{a}} = -e_{\mathrm{c}} = E$ (E is denoted as phase back EMF amplitude). According to (2), the electromagnetic torque $T_{\mathrm{e-noc}}$ during the normal conduction period is expressed as

$$T_{\mathrm{e-noc}} = \frac{e_{\mathrm{a}}i_{\mathrm{a}} + e_{\mathrm{b}}i_{\mathrm{b}} + e_{\mathrm{c}}i_{\mathrm{c}}}{\omega_{\mathrm{m}}} = -\frac{2Ei_{\mathrm{c}}}{\omega_{\mathrm{m}}}. \tag{3}$$

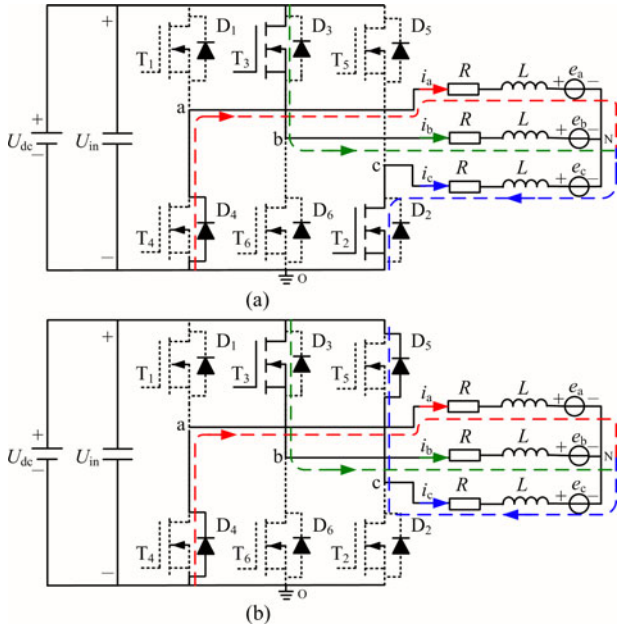

Fig. 3. Currents of three-phase windings in the commutation process from "a$^+$c$^-$" to "b$^+$c$^-$". (a) MOSFET T_2 is ON. (b) MOSFET T_2 is OFF.

During the commutation period, there are currents in all the three-phase stator windings due to the inductance of the stator windings, and the actual phase current cannot be a rectangular wave shown in Fig. 2. Take the commutation of the motor from "a$^+$c$^-$" to "b$^+$c$^-$" as an example. The back EMFs are almost constant as the duration of commutation is short, and then $e_a = e_b = -e_c = E$. Based on the Kirchhoff's law $i_a + i_b + i_c = 0$, according to (2), the electromagnetic torque T_{e-com} during the commutation period is given by

$$T_{e-com} = \frac{e_a i_a + e_b i_b + e_c i_c}{\omega_m} = -\frac{2Ei_c}{\omega_m}. \tag{4}$$

According to (3) and (4), the torque ripple can be reduced by keeping the noncommutated current i_c steady, which can be achieved by the proper PWM method. To avoid switching modulation methods, the same modulation method is adopted during both the normal conduction period and commutation period, and the PWM is applied to the noncommutated phase MOSFET during the commutation period. By taking the commutation from "a$^+$c$^-$" to "b$^+$c$^-$" as an example, Fig. 3 shows the currents in three-phase windings during the commutation period.

As shown in Fig. 3, the outgoing phase current flows through the freewheeling diode D_4 and the MOSFET T_3 is ON, and the PWM is applied to the MOSFET T_2. Ignoring the voltage drop of the freewheeling diode, the three-phase terminal voltages of BLDCM during the commutation period are expressed as

$$\begin{cases} 0 = Ri_a + L\frac{di_a}{dt} + E + U_{No} \\ U_{in} = Ri_b + L\frac{di_b}{dt} + E + U_{No} \\ (1-d)U_{in} = Ri_c + L\frac{di_c}{dt} - E + U_{No} \end{cases} \tag{5}$$

where d is the duty cycle of T_2, and U_{in} is the input voltage of three-phase bridge inverter.

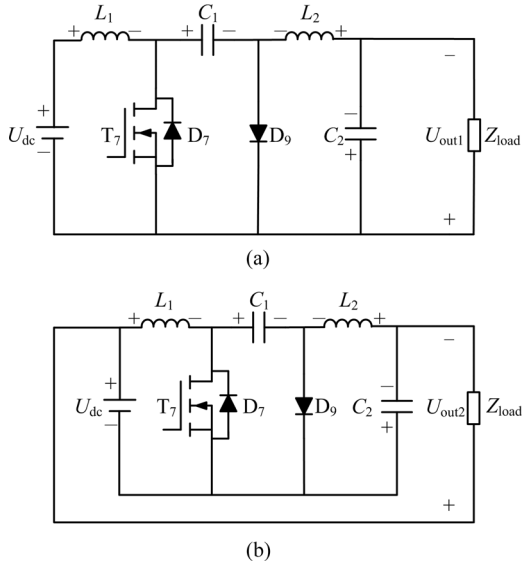

Fig. 4. Two output modes of Cuk converter. (a) Cuk converter in buck–boost mode. (b) Cuk converter in boost mode.

By adding the equations in (5) together and considering $i_a + i_b + i_c = 0$, the average neutral point voltage U_{No} can be derived as

$$U_{No} = \frac{(2-d)U_{in} - E}{3}. \tag{6}$$

According to the third equation in (5) and (6), the noncommutated current rate of change is derived as

$$\frac{di_c}{dt} = \frac{(1-2d)U_{in} + 4E - 3Ri_c}{3L}. \tag{7}$$

By setting (7) as zero to keep the noncommutated current steady, the duty cycle d can be obtained as

$$d = 0.5 + \frac{4E - 3i_c R}{2U_{in}}. \tag{8}$$

According to (8), since $0 \le d \le 1$, d is the upper threshold 1 and $di_c/dt \neq 0$ when $4E - 3i_c R \ge U_{in}$. In other words, the commutation torque ripple cannot be effectively reduced in the high speed range with the finite input voltage of three-phase bridge inverter. If the input voltage of the inverter satisfies $U_{in} \ge 4E - 3i_c R$ during the commutation period, the commutation torque ripple will be reduced effectively in the high speed range.

III. Different Output Modes of Cuk Converter

The Cuk converter has different output voltages for different output modes. The Cuk converters in the buck–boost mode and the boost mode are shown in Fig. 4(a) and (b), respectively.

The operational principle of the Cuk converter is analyzed as following. The equivalent circuits of the Cuk converter in the buck–boost mode with T_7 being ON and OFF are shown in Fig. 5.

Fig. 5(a) illustrates the equivalent circuit of the Cuk converter in the buck–boost mode, in which the MOSFET T_7 is ON and the diode D_9 is OFF. Meanwhile, the inductors L_1 and L_2 store

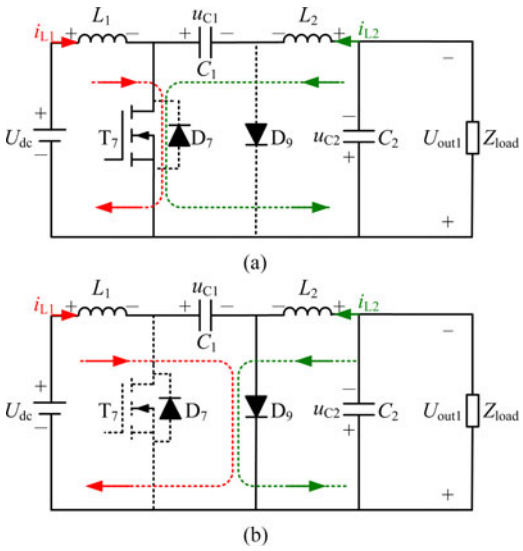

Fig. 5. The equivalent circuits of the Cuk converter in the buck–boost mode. (a) MOSFET T_7 is ON. (b) MOSFET T_7 is OFF.

energy, and we have

$$\begin{cases} L_1 \frac{\mathrm{d}i_{L1}}{\mathrm{d}t} = U_{\mathrm{dc}} \\ L_2 \frac{\mathrm{d}i_{L2}}{\mathrm{d}t} = u_{C1} - u_{C2} \end{cases} \tag{9}$$

where i_{L1} and i_{L2} are the currents flowing through the inductors L_1 and L_2, respectively, and u_{C1} and u_{C2} are the voltages of the capacitances C_1 and C_2 respectively.

Fig. 5(b) illustrates the equivalent circuit of the Cuk converter in the buck–boost mode, in which the MOSFET T_7 is OFF and the diode D_9 is ON. Meanwhile, the inductors L_1 and L_2 release energy, and ignoring the voltage drop of the freewheeling diode, we have

$$\begin{cases} L_1 \frac{\mathrm{d}i_{L1}}{\mathrm{d}t} = U_{\mathrm{dc}} - u_{C1} \\ L_2 \frac{\mathrm{d}i_{L2}}{\mathrm{d}t} = -u_{C2} \end{cases}. \tag{10}$$

Within a modulation period T_s, the average voltages of the inductors L_1 and L_2 are both zero. According to (9) and (10), we have

$$\begin{cases} d_c U_{\mathrm{dc}} + (1-d_c)(U_{\mathrm{dc}} - U_{C1}) = 0 \\ d_c(U_{C1} - U_{C2}) - (1-d_c)U_{C2} = 0 \end{cases} \tag{11}$$

where d_c is the duty cycle of the MOSFET T_7, and U_{C1} and U_{C2} are the average voltages of the capacitances C_1 and C_2, respectively. By (11), we have

$$\begin{cases} U_{C1} = \frac{U_{\mathrm{dc}}}{1-d_c} \\ U_{C2} = d_c U_{C1} \end{cases}. \tag{12}$$

From Fig. 5 and (12), the output voltage U_{out1} of the Cuk converter in the buck–boost mode is derived as

$$U_{\mathrm{out1}} = U_{C2} = \frac{d_c U_{\mathrm{dc}}}{1-d_c}. \tag{13}$$

By making a comparison between Fig. 4(a) and (b), it is known that the two different output modes have the same operational principle. In other words, the formulas (9)–(12) are also applicable to the Cuk converter in the boost mode, in which the output voltage U_{out2} of the Cuk converter is obtained from Fig. 4(b) as

$$U_{\mathrm{out2}} = U_{\mathrm{dc}} + U_{C2} = \frac{U_{\mathrm{dc}}}{1-d_c}. \tag{14}$$

From the aforesaid analysis, the Cuk converter in different output modes has the different output voltages with the same operational principle. Moreover, the output voltage of the Cuk converter in the boost mode U_{out2} is always larger than the power supply voltage U_{dc}, which provides the possibility to step up the input voltage of the three-phase bridge inverter.

IV. Proposed Strategy to Reduce the Commutation Torque Ripple

The Cuk converter can be used to supply power for the BLDCM as it has two different output voltages with different output modes, and the commutation torque ripple can be reduced by altering the output modes of the converter. The block diagram of the proposed commutation torque ripple reduction strategy in this paper is presented in Fig. 6, where the control unit contains the control to alter the output modes of the Cuk converter, the voltage control of the Cuk converter during the normal conduction period, the noncommutated phase current stable strategy during the commutation period, and the detection module. The control to alter the output modes of the Cuk converter is realized by a designed mode selection circuit, and during the commutation period the output modes are altered to step up the input voltage of three-phase bridge inverter and then meet the voltage demand of commutation period. The voltage control of the Cuk converter is achieved by adopting the speed and current double closed-loop control strategy during the normal conduction period, which can regulate the input voltage of the inverter to meet the speed adjustment of the motor. The noncommutated phase current stable strategy is used to keep the noncommutated phase current steady and then reduce the commutation torque ripple. In the detection module, the start of commutation is triggered by the change of hall signals, and the commutation comes to an end when the outgoing current reduces to zero.

A. Control to Alter the Output Modes of the Cuk Converter

A mode selection circuit shaded in Fig. 6 is designed to alter the output modes of the converter in this paper. The circuit consists of MOSFET T_c and diode D_8 with complementary conduction state, which can alter the output modes of the Cuk converter by the turn-on/off of T_c. Since the two output modes are both to supply power for the BLDCM, different input voltages of the inverter U_{in} is obtained.

As shown in Fig. 7(a), during the normal conduction period, Cuk converter operates in the buck–boost mode with MOSFET T_c being OFF and diode D_8 being ON. Meanwhile, the Cuk converter supplies power for the BLDCM via the diode D_8 and the three-phase bridge inverter. Ignoring the voltage drop of the MOSFET and diode, the input voltage of the inverter U_{in} is expressed as (13).

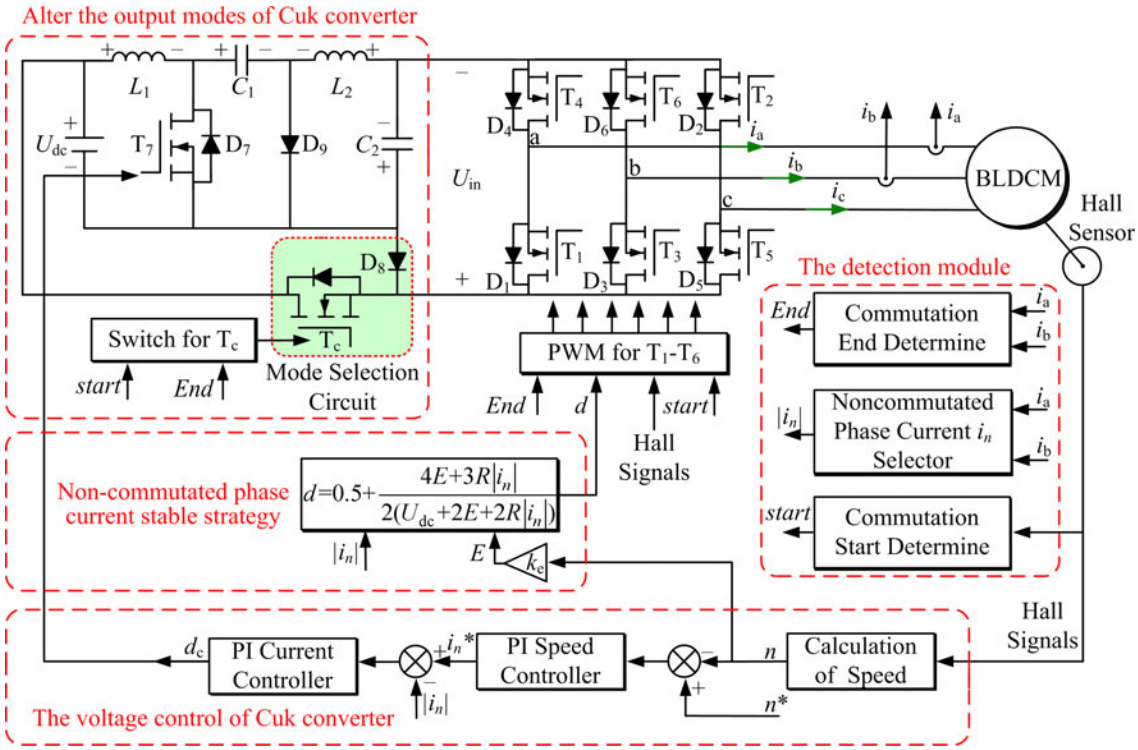

Fig. 6. Block diagram of the proposed commutation torque ripple reduction strategy.

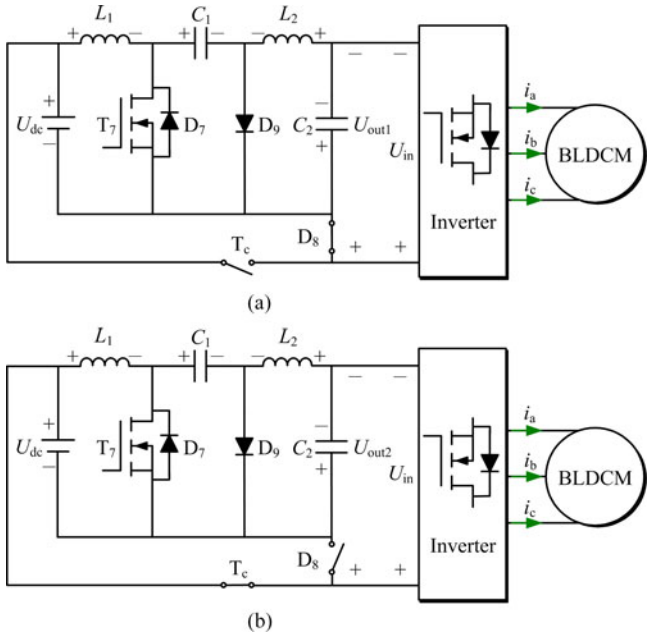

Fig. 7. Switch states of T_c in the mode selection circuit and the output modes of Cuk converter. (a) Cuk converter in the buck–boost mode during the normal conduction period. (b) Cuk converter in the boost mode during the commutation period.

As shown in Fig. 7(b), during the commutation period, in order to step up the input voltage of the inverter and keep the noncommutated phase current steady, Cuk converter operates in the boost mode with MOSFET T_c being ON and diode D_8 being OFF. Meanwhile, the Cuk converter supplies power for the BLDCM via the MOSFET T_c and the three-phase bridge inverter. Ignoring the voltage drop of the MOSFET and diode, the input voltage of the inverter U_{in} is expressed as (14).

B. Voltage Control of Cuk Converter During the Normal Conduction Period

The demand of the motor speed adjustment can be met by the PWM chopping of the inverter when the power supply voltage is constant, take a^+c^- as an example. By the first and the third equations of (1), the line voltage of two conducting phases during the normal conduction period u_{ac} can be obtained as

$$u_{ac} = u_a - u_c = -2Ri_c - 2L\frac{di_c}{dt} + 2E. \tag{15}$$

Within a modulation period T_s, the phase current i_c is almost unchanged, and then the average line voltage of two conducting phases U_{ac} is derived as

$$U_{ac} = \overline{u}_{ac} = -2Ri_c + 2E = d_n U_{in} \tag{16}$$

where d_n is the duty cycle of T_1, by (16), we have

$$d_n = \frac{-2Ri_c + 2E}{U_{in}}. \tag{17}$$

Compared with the method in [16], speed regulation can be realized by either PWM chopping of the three-phase inverter with constant input voltage or PAM control of the Cuk converter in this paper. When the PAM method is adopted, the voltage spike caused by turn-on/off of MOSFET in the three-phase inverter and the current ripple generated by high-frequency PWM

chopping are both reduced, and the program of the modulation method is also simplified further [25], [26].

In this paper, during the normal conduction period, the input voltage of the inverter is regulated by the PAM method of Cuk converter in the buck–boost mode instead of the PWM chopping of the inverter, namely, $d_{\rm n} = 1$ in (17). Under the two-phase conduction mode with six steps commutation, the input voltage of the inverter is given by

$$U_{\rm in} = U_{\rm out1} = 2R\,|i_n| + 2E \tag{18}$$

where i_n is noncommutated current. By (13) and (18), the duty cycle $d_{\rm c}$ of T_7 during the normal conduction period is derived as

$$d_{\rm c} = \frac{2R\,|i_n| + 2E}{U_{\rm dc} + 2R\,|i_n| + 2E}. \tag{19}$$

During the normal conduction period, MOSFET $T_{\rm c}$ is OFF and Cuk converter is in the buck–boost mode, and the detail control method can be seen in Fig. 6. The reference speed of the PI speed controller n^* is given by the upper computer and the rotor speed calculated by three hall sensors is the feedback of the speed controller. The reference current of the PI current controller is the output of the speed controller and the feedback of the current controller is the sampled noncommutated current i_n. Then, the input voltage control of the inverter can be achieved by adjusting the output duty cycle $d_{\rm c}$ of the current controller.

C. Noncommutated Phase Current Stable Strategy During Commutation Period

In order to reduce the commutation torque ripple, the MOSFET $T_{\rm c}$ in the mode selection circuit turns on and the Cuk converter operates in the boost mode when the start of commutation is triggered by the change of hall signals. Besides, the duty cycle of MOSFET T_7 during the whole commutation period is the one in a previous modulation period before the commutation. As shown in Fig. 7(b), the input voltage of the inverter is represented as

$$U_{\rm in} = U_{\rm out2} = U_{\rm out1} + U_{\rm dc} = 2E + 2R\,|i_n| + U_{\rm dc}. \tag{20}$$

Since $U_{\rm dc} \geq 2E + 2R|i_n|$ ($U_{\rm dc}$ is the rated voltage) when the BLDCM operates below rated operation condition, the relationship $U_{\rm in} \geq 4E + 3R|i_n|$ can be satisfied during the commutation period based on (20). In other words, the output voltage of the Cuk converter in the boost mode is larger than the required input voltage of the inverter. According to (8) and (20), to keep the noncommutated phase current steady, the duty cycle of MOSFET applied to the noncommutated phase during the commutation period is derived as

$$d = 0.5 + \frac{4E + 3\,|i_n|\,R}{2(U_{\rm dc} + 2E + 2\,|i_n|\,R)}. \tag{21}$$

When the outgoing current reduces to zero, the commutation comes to an end and the MOSFET $T_{\rm c}$ turns off; meanwhile, the control strategy of the normal conduction period is resumed.

Fig. 8 illustrates the modulation method of the proposed commutation torque ripple reduction strategy. During the normal conduction period, MOSFET $T_{\rm c}$ is OFF and Cuk converter is in the buck–boost mode. The input voltage of the inverter is regulated by adopting the speed and current closed-loop control strategy, which can achieve the speed adjustment of the motor without the PWM chopping of the inverter. During the commutation period, MOSFET $T_{\rm c}$ is ON and Cuk converter is in the boost mode. The input voltage of the inverter can meet the voltage demand of the commutation period, and the noncommutated current can be kept steady by adjusting the duty cycle of MOSFET applied to the noncommutated phase. When the outgoing current reduces to zero, the commutation comes to an end and MOSFET $T_{\rm c}$ turns OFF, meanwhile, the control strategy of the normal conduction period is resumed.

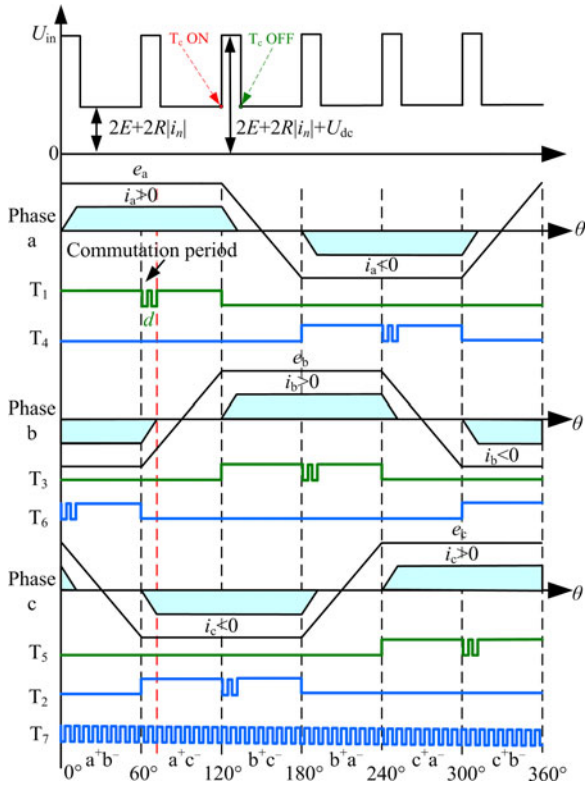

Fig. 8. Modulation method diagram of the proposed commutation torque ripple reduction strategy.

V. Implementation and Experimental Results

The experimental prototype shown in Fig. 9 is built to verify the correctness of the theory and the effectiveness of the proposed method.

In the prototype, the core processor is TMS320F28335 produced by TI Company with 150MHz clock frequency, and the MOSFET is IRFB4030PbF produced by International Rectifier. Besides, two current sensors are used to measure the phase currents $i_{\rm a}$ and $i_{\rm b}$. The basic parameters of the BLDCM and the Cuk converter are listed in Table I.

The experimental prototype is supplied by an Agilent N5767A DC source. The experimental results are recorded by a digital oscilloscope DLM2024 with a logic probe PBL100 to acquire the switching signals of the three-phase bridge inverter,

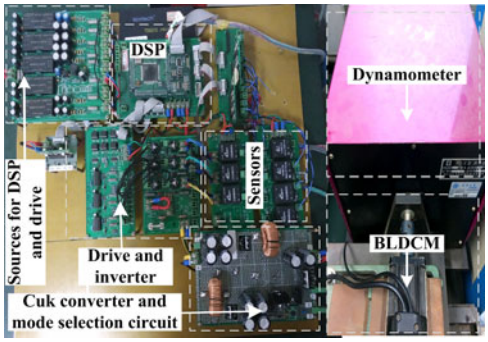

Fig. 9. Experiment prototype.

TABLE I
PARAMETERS OF BLDCM AND CUK CONVERTER

Parameters	Value	Unit
Rated voltage U_N	24	V
Rated power P_N	70	W
Rated current I_N	4	A
Rated load T_N	0.23	N·m
Rated speed n_N	3000	r/ min
Phase Back EMF coefficient k_e	0.028	V/ (rad/ s)
Pairs of poles p	5	
Phase resistance R	0.33	Ω
Phase inductance L	0.61	mH
Cuk capacitance C_1	1100	μF
Cuk capacitance C_2	2200	μF
Cuk inductance L_1	330	μH
Cuk inductance L_2	330	μH

the driving signal T_7 of the Cuk converter, and the switching signal T_c of the mode selection circuit. The load of the BLDCM is provided by a dynamometer that can display the speed of BLDCM in real time.

By (3) and (4), whether it is the commutation period or the normal conduction period, the electromagnetic torque is proportional to the noncommutated phase current. Therefore, the electromagnetic torque ripple can be approximately equivalent to the noncommutated current ripple, and the current ripple rate I_{rt} is defined as

$$I_{rt} = \frac{I_{high} - I_{low}}{I_{high} + I_{low}} \times 100\% \tag{22}$$

where I_{high} and I_{low} are the maximum and minimum current over a period of time, respectively.

For comparison, the BLDCM is driven by a voltage-source inverter with the ON-PWM modulation method in the traditional strategy, in which the speed and current double closed-loop control strategy is adopted. To verify the performance of the proposed strategy under rated operating condition, Fig. 10(a) and (b) show the experimental results of the traditional strategy and the proposed strategy with the speed reference value being 3000 r/min and the load torque being 0.23 N·m. Each figure from top to bottom is mechanical torque, three phase currents, the input voltage of the inverter U_{in}, and PWM signals of phase "a". For the proposed strategy in this paper, the driving signal T_7 of the Cuk converter and the switching signal T_c of the

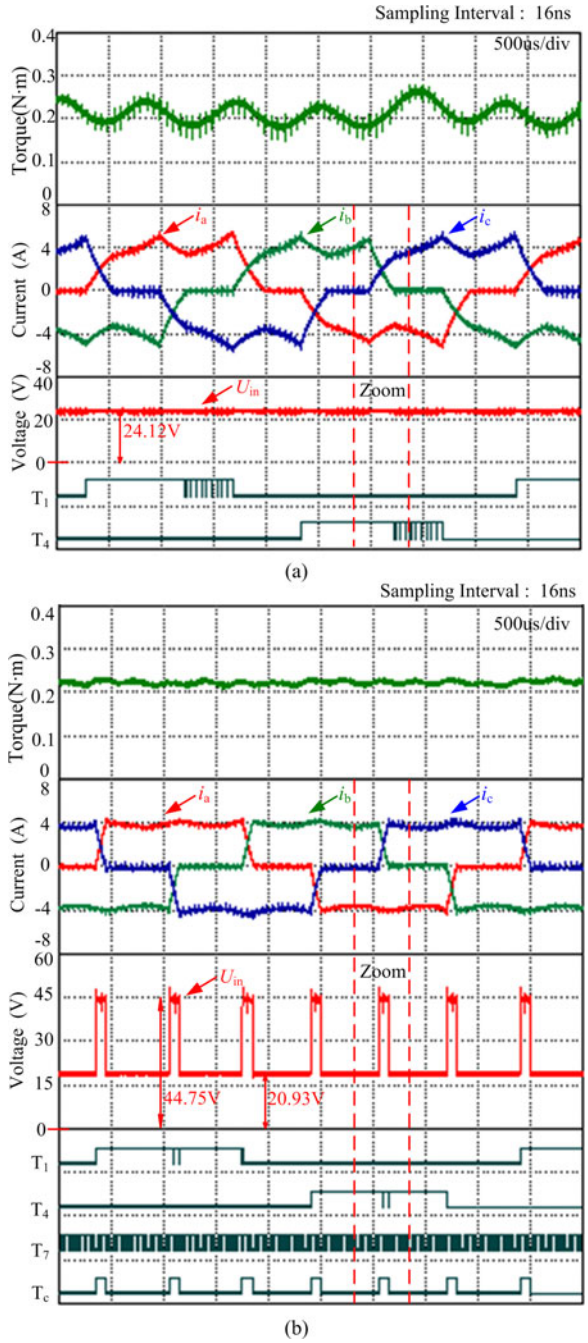

Fig. 10. Experimental results with the speed being 3000 r/min and the load being 0.23 N·m. (a) Traditional control strategy. (b) Proposed commutation torque ripple reduction strategy.

mode selection circuit (high level indicates T_c is ON) are also displayed in Fig. 10(b).

As shown in Fig. 10, significant fluctuation of the noncommutated phase current can be found in the traditional strategy with I_{rt} being 37.3%, while the remarkable reduction of the noncommutated current fluctuation can be found in the proposed strategy with I_{rt} being only 7.2%.

The details of the two methods in the commutation process are shown in Fig. 11(a) and (b), respectively. From Fig. 11(a), during the commutation period, the finite input voltage of the

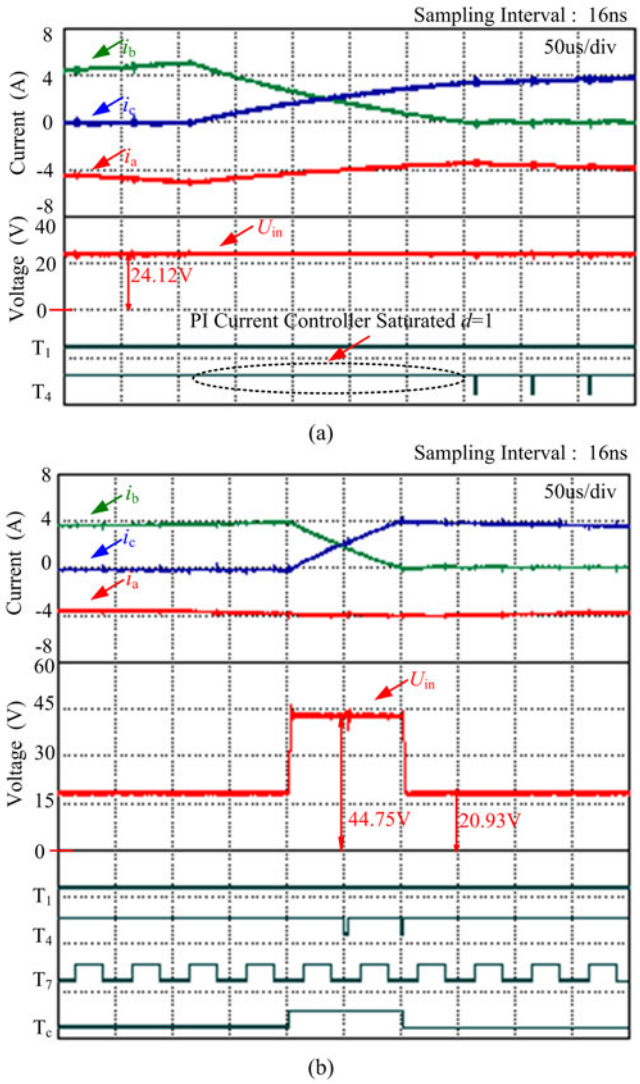

Fig. 11. Details of experimental results with the speed being 3000 r/ min and the load being 0.23 N·m during the commutation period. (a) Traditional control strategy. (b) Proposed commutation torque ripple reduction strategy.

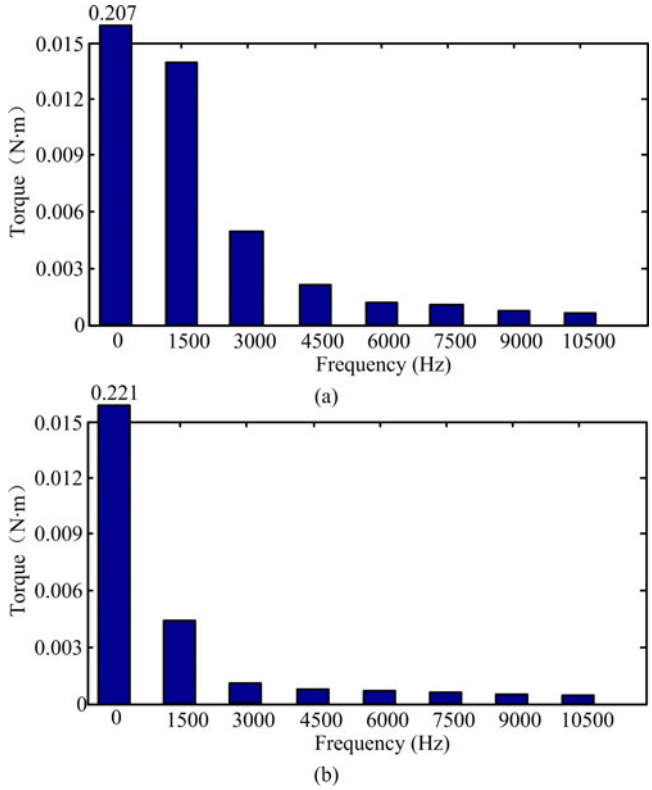

Fig. 12. Harmonic spectra of mechanical torque with the speed being 3000 r/min and the load torque being 0.23 N·m. (a) Traditional method. (b) Proposed method.

inverter makes the PI current controller saturated in the traditional strategy, and the duty cycle applied to the MOSFET of the noncommutated phase reaches the upper threshold 1. From Fig. 11(b), in the proposed strategy, once the commutation signal is detected, the MOSFET T_c of the mode selection circuit turns ON and the Cuk converter operates in the boost mode to step up the input voltage of the inverter. Then, keeping the noncommutated phase current steady can be achieved by the PWM applied to the MOSFET of the noncommutated phase.

The torque harmonic causing the vibration in motors is the main source of noises, and the harmonic analysis of mechanical torque waveform is made. Fig. 12(a) and (b) show the harmonic analysis results of the traditional strategy and the proposed strategy with the speed being 3000 r/ min and the load torque being 0.23 N·m.

When the motor operates at 3000 r/min, the fundamental frequency of phase current is $f = 3000p/60 = 250$ Hz. The torque harmonic caused by commutation is integer times of commutation frequency 6*f*. From Fig. 12(a), the harmonic component with integer times of 6*f* is larger in the traditional method, where the harmonic amplitudes at 6*f* and 12*f* are 0.0142 and 0.0054, respectively. From Fig. 12(b), the harmonic component with integer times of 6*f* is reduced significantly in the proposed method, where the harmonic amplitudes of 6*f* and 12*f* are 0.0044 and 0.0008, respectively. The results show that the proposed method can effectively suppress the commutation torque ripple. Fig. 12(b) shows the torque harmonic with 1500 Hz still exists to some extent, whereas it is caused by the cogging torque which can be reduced by a reasonable optimization of motor design. In addition, nonideal EMF has little influence on the torque harmonic, so it is not considered in this paper.

To verify the performance of the proposed strategy under low-speed condition, Fig. 13(a) and 13(b) show the experimental results of the traditional strategy and the proposed strategy with the speed reference value being 500 r/min and the load torque being 0.23 N·m.

As shown in Fig. 13, significant fluctuation of the noncommutated phase current can be also found in the traditional strategy with I_{rt} being 32.6%, while the remarkable reduction of the noncommutated current fluctuation can be found in the proposed strategy with I_{rt} being only 9.4%. Besides, From Fig. 13(a) and (b), in the proposed strategy, during the normal conduction period, the input voltage of the inverter is adjusted by utilizing the PAM method without PWM chopping of the

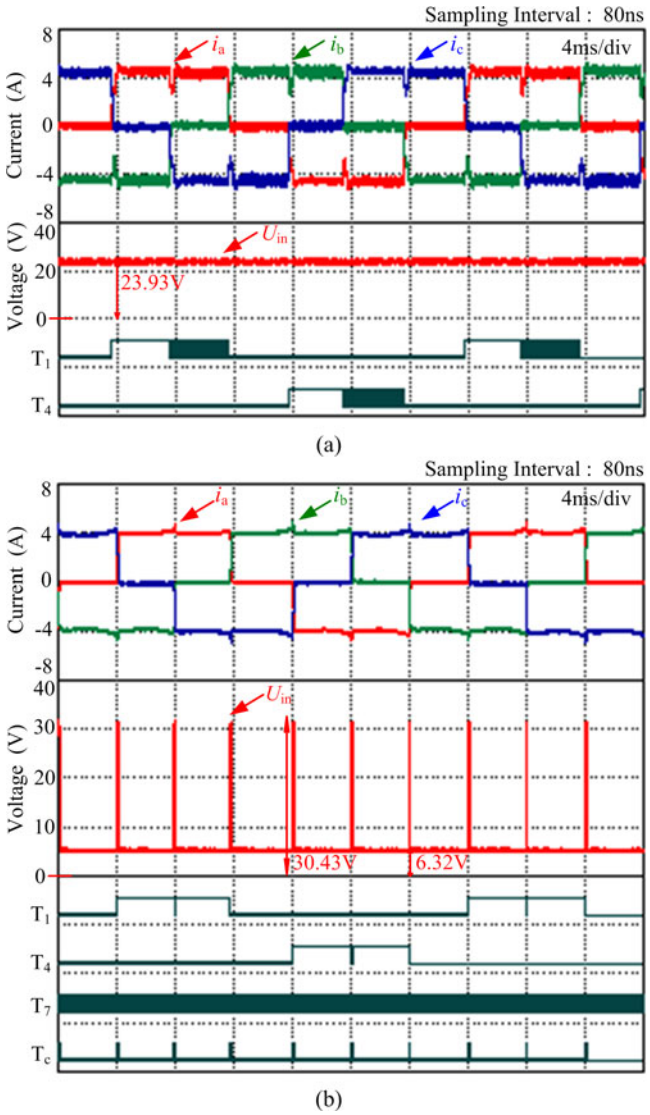

Fig. 13. Experimental results with the speed being 500 r/min and the load being 0.23 N·m. (a) Traditional control strategy. (b) Proposed commutation torque ripple reduction strategy.

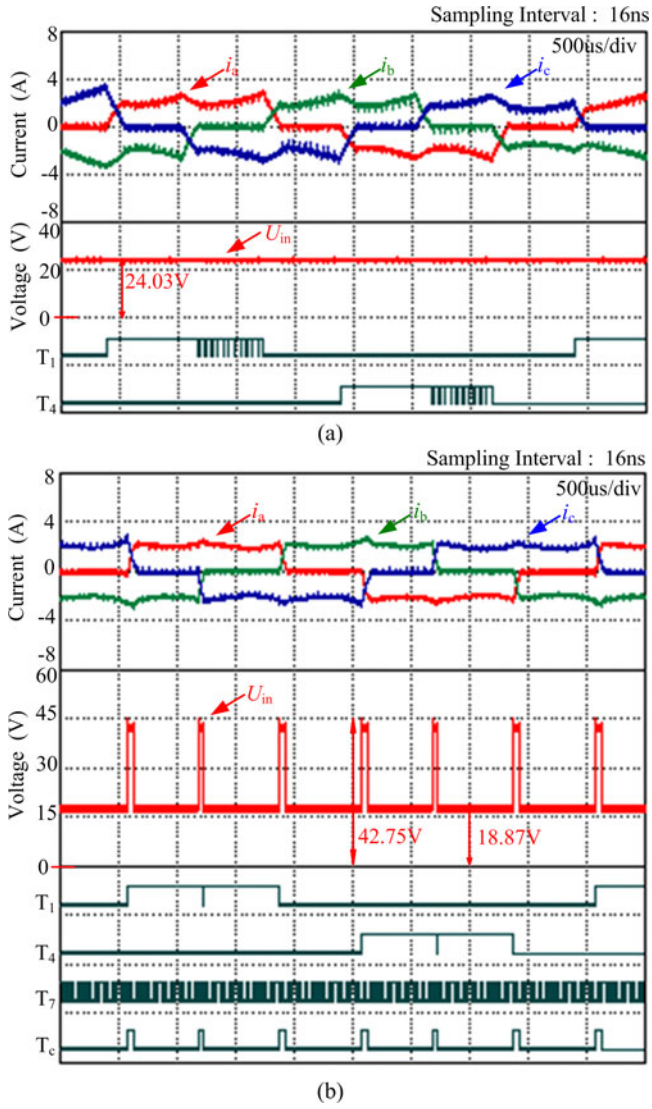

Fig. 14. Experimental results with the speed being 3000 r/min and the load being 0.11 N·m. (a) Traditional control strategy. (b) Proposed commutation torque ripple reduction strategy.

inverter, which reduces the high-frequency interference caused by the turn-on/off of MOSFET in the three-phase bridge inverter and then achieves the smoother current.

To verify the performance of the proposed strategy under light load condition, Fig. 14(a) and (b) show the experimental results of the two methods with the speed reference value being 3000 r/min and the load torque being 0.11 N·m.

As shown in Fig. 14, significant fluctuation of the noncommutated phase current can be found in the traditional strategy with I_{rt} being 28.5%, while the remarkable reduction of the noncommutated current fluctuation can be found in the proposed strategy with I_{rt} being only 10.7%.

In order to verify the speed response performance of the proposed method, reference speed n^* follows ramp function during experimental process. Fig. 15(a) and (b) represent the dynamic response of speed variation and its enlarged vision, respectively.

BLDCM operates at 500 r/min with 0.1 N·m load torque before acceleration. During acceleration process, the reference speed follows ramp function, and the speed is raised to 3000 r/ min in 2 s. It can be found from Fig. 15(a) that the output voltage U_{out1} of the Cuk converter increases along the ramp during acceleration, and the actual speed of BLDCM n follows its reference value n^* accurately. Experimental results show that the proposed method has good dynamic performance with speed variation.

Fig. 15(b) shows the zoom of speed dynamic response. The results illustrate that the proposed torque ripple reduction strategy can keep the noncommutated phase current steady when speed varies. That is because back EMF E can be obtained from motor speed n, and noncommutated phase current i_n can be measured by current sensor in the process of acceleration. Thus, commutation torque ripple can be reduced effectively.

In order to verify the dynamic performance of load torque change, experiments with load torque change are carried out.

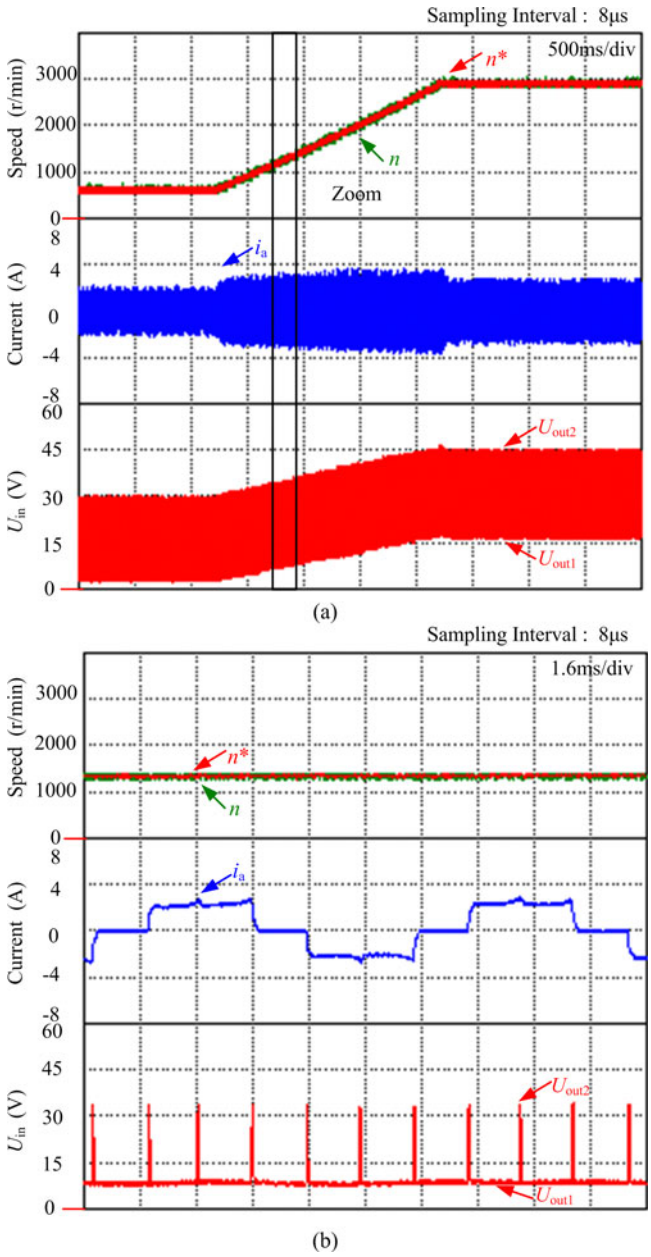

Fig. 15. Dynamic response of speed variation in the proposed method. (a) Speed, current, and input voltage of three-phase inverter. (b) Zoom of the speed dynamic response.

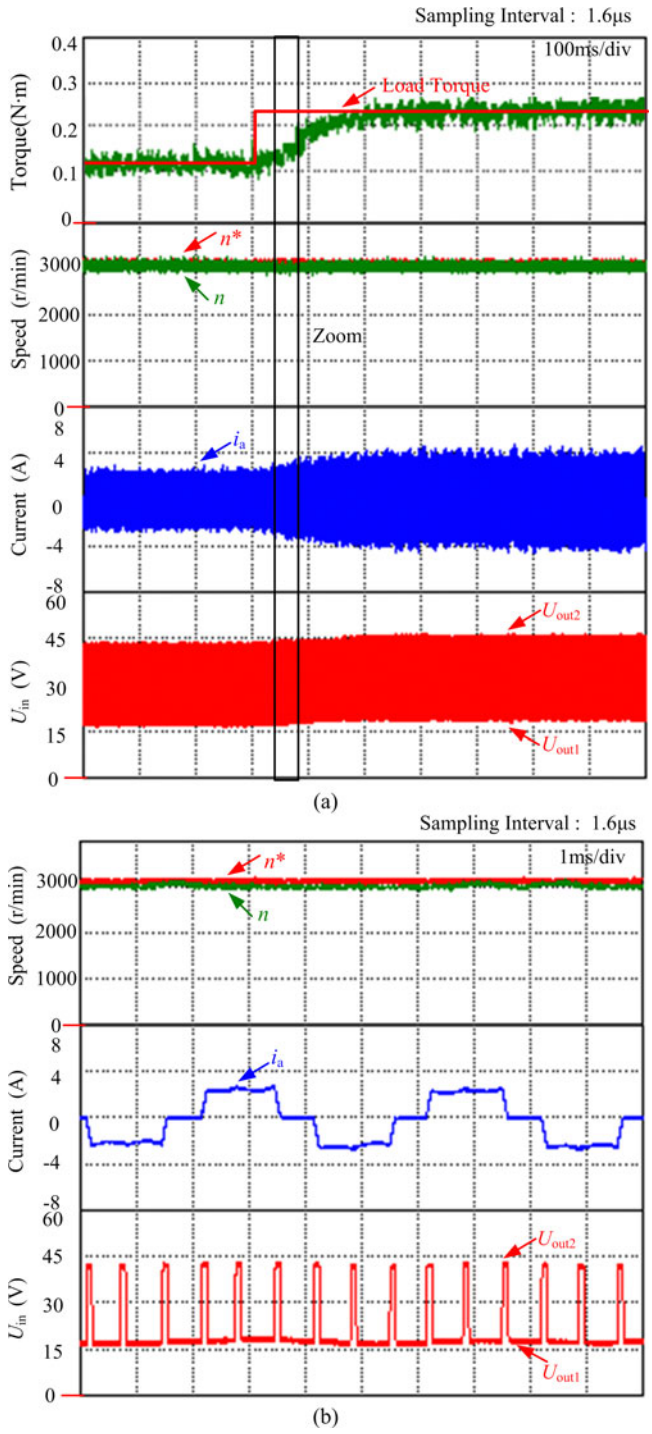

Fig. 16. Dynamic response of load torque change. (a) Torque, speed, current, and input voltage of three-phase inverter. (b) Zoom of the torque dynamic response.

Fig. 16(a) and (b) show the dynamic response of load torque change and its enlarged vision, respectively.

BLDCM operates at 3000 r/ min with 0.11 N·m before the load torque is abruptly increased. During the experimental process, load torque steps up from 0.11 to 0.23 N·m. It can be seen from Fig. 16(a) that phase current increases with load torque increasing, and the output voltage U_{out1} of the Cuk converter is also increased to maintain the motor speed steady. Experimental results show that the proposed scheme can handle the situation of load torque change effectively, and has good dynamic performance.

Fig. 16(b) is the zoom of load torque dynamic response. The results show that the proposed torque ripple reduction strategy can keep the non-commutated phase current steady when load torque changes. That is because back EMF E can be obtained from motor speed n, and noncommutated phase current i_n can be measured by current sensor in the dynamic process. Thus, commutation torque ripple can be reduced effectively.

It is noted that MOSFET $\mathrm{T_c}$ is required to be turned on and turned off at the beginning and end moment of commutation

in the proposed method to reduce commutation torque ripple. Meanwhile, PWM chopping is carried out in commutation period. For high-speed BLDCM, common mode noises would be introduced to some extent. Nevertheless, commutation time is very short for high-speed BLDCM, so the common mode noises are limited. In addition, for conditions having strict demands for common mode noises, the noises can be reduced effectively by designing EMC [27], [28].

VI. Conclusion

This paper proposes a novel commutation torque ripple reduction strategy of the Cuk converter fed BLDCM. In the proposed method, during the commutation period, the output modes of the Cuk converter are altered by the designed mode selection circuit to step up the input voltage of three-phase bridge inverter, such that the commutation torque ripple can be reduced by keeping the noncommutated current steady over the entire speed range.

In conclusion, the proposed approach has the following advantages:

1) In this paper, the Cuk converter operates in two different output modes by a designed mode selection circuit and different input voltages of the three-phase bridge inverter is obtained, which provides the possibility to step up the input voltage of the inverter and then meet the voltage demand of the commutation period.
2) The proposed method can effectively reduce the commutation torque ripple over the entire speed range, which avoids the switch of modulation methods between high speed and low speed that may reduce the system stability, and simplifies the program of modulation method.
3) Since the inverter PWM chopping is not required during the normal conduction period, the voltage spike damage to the motor windings caused by turn-on/off of MOSFET in the inverter is reduced, and the utilization of the Cuk converter is enhanced.

References

[1] Z. Q. Zhu and J. H. Leong, "Analysis and mitigation of torsional vibration of PM brushless AC/DC drives with direct torque controller," *IEEE Trans. Ind. Appl.*, vol. 48, no. 4, pp. 1296–1306, Jul./Aug. 2012.

[2] J. Zou, W. Qi, Y. Xu, F. Xu, and J. Li, "Design of deep sea oil-filled brushless DC motors considering the high pressure effect," *IEEE Trans. Magn.*, vol. 48, no. 11, pp. 4220–4223, Nov. 2012.

[3] J. Fang, W. Li, and H. Li, "Self-compensation of the commutation angle based on dc-link current for high-speed brushless DC motors with low inductance," *IEEE Trans. Power Electron.*, vol. 29, no. 1, pp. 428–438, Jan. 2014.

[4] R. Carlson, M. Lajoie-Mazenc, and J. C. D. S. Fagundes, "Analysis of torque ripple due to phase commutation in brushless DC machines," *IEEE Trans. Ind. Appl.*, vol. 28, no. 3, pp. 632–638, May/Jun. 1992.

[5] C. L. Xia, Y. W. Xiao, W. Chen, and T. N. Shi, "Torque ripple reduction in brushless DC drives based on reference current optimization using integral variable structure control," *IEEE Trans. Ind. Electron.*, vol. 61, no. 2, pp. 738–752, Feb. 2014.

[6] Y. Liu, Z. Q. Zhu, and D. Howe, "Commutation-torque-ripple minimization in direct-torque-controlled PM brushless DC drives," *IEEE Trans. Ind. Appl.*, vol. 43, no. 4, pp. 1012–1021, Jul./Aug. 2007.

[7] J. H. Song and I. Choy, "Commutation torque ripple reduction in brushless DC motor drives using a single dc current sensor," *IEEE Trans. Power Electron.*, vol. 19, no. 2, pp. 312–319, Mar. 2004.

[8] J. Shi and T. C. Li, "New method to eliminate commutation torque ripple of brushless DC motor with minimum commutation time," *IEEE Trans. Ind. Electron.*, vol. 60, no. 6, pp. 2139–2146, Jun. 2013.

[9] H. Lu, L. Zhang, and W. Qu, "A new torque control method for torque ripple minimization of BLDC motors with un-ideal back EMF," *IEEE Trans. Power Electron.*, vol. 23, no. 2, pp. 950–958, Mar. 2008.

[10] J. Fang, X. Zhou, and G. Liu, "Instantaneous torque control of small inductance brushless DC motor," *IEEE Trans. Power Electron.*, vol. 27, no. 12, pp. 4952–4964, Dec. 2012.

[11] Y. K. Lin and Y. S. Lai, "Pulsewidth modulation technique for BLDCM drives to reduce commutation torque ripple without calculation of commutation time," *IEEE Trans. Ind. Appl.*, vol. 47, no. 4, pp. 1786–1793, Jul/Aug. 2011.

[12] D. K. Kim, K. W. Lee, and B. I. Kwon, "Commutation torque ripple reduction in a position sensorless brushless DC motor drive," *IEEE Trans. Power Electron.*, vol. 21, no. 6, pp. 1762–1768, Nov. 2006.

[13] Y. Wei, Y. Xu, J. Zou, K. Liu, and H. Wang, "Analytic investigation on commutation angle of brushless DC motors with 120 voltage source inverter," *Int. J. Appl. Electromagnet Mech.*, vol. 45, pp. 219–225, 2014.

[14] Y. Xu, Y. Wei, B. Wang, and J. Zou, "A novel inverter topology for brushless DC motor drive to shorten commutation time," *IEEE Trans. Ind. Electron.*, vol. 63, no. 2, pp. 796–807, Feb. 2016.

[15] X. M. Li, C. L. Xia, Y. F. Cao, W. Chen, and T. N. Shi, "Commutation torque ripple reduction strategy of Z-source inverter fed brushless DC motor," *IEEE Trans. Power Electron.*, vol. 31, no. 11, pp. 7677–7690, Nov. 2016.

[16] T. N. Shi, Y. T. Guo, P. Song, and C. L. Xia, "A new approach of minimizing commutation torque ripple for brushless DC motor based on DC-DC converter," *IEEE Trans. Ind. Electron.*, vol. 57, no. 10, pp. 3483–3490, Oct. 2010.

[17] S. Cuk and R. D. Middlebrook, "A general unified approach to modelling switching dc-to-dc converters in discontinuous conduction mode," in *Proc. IEEE Power Electron. Spec. Conf.*, 1977, pp. 36–57.

[18] V. Bist and B. Singh, "PFC Cuk converter-fed BLDC motor drive," *IEEE Trans. Power Electron.*, vol. 30, no. 2, pp. 871–887, Feb. 2015.

[19] M. Zhu and F. L. Luo, "Enhanced self-lift Cûk converter for negative-to-positive voltage conversion," *IEEE Trans. Power Electron*, vol. 25, no. 9, pp. 2227–2233, Sep. 2010.

[20] I. O. Lee, S. Y. Cho, and G. W. Moon, "Interleaved buck converter having low switching losses and improved step-down conversion ratio," *IEEE Trans. Power Electron*, vol. 27, no. 8, pp. 3664–3675, Aug. 2012.

[21] C. T. Pan and C. M. Lai, "A high-efficiency high step-up converter with low switch voltage stress for fuel-cell system applications," *IEEE Trans. Ind. Electron.*, vol. 57, no. 6, pp. 1998–2006, Jun. 2010.

[22] Z. Chen, "PI and sliding mode control of a Cuk converter," *IEEE Trans. Power Electron.*, vol. 27, no. 8, pp. 3695–3703, Aug. 2012.

[23] P. K. Singh, Y. V. Hote, and M. M. Garg, "Comments on "PI and sliding mode control of a cuk converter," *IEEE Trans. Power Electron.*, vol. 29, no. 3, pp. 1551–1552, Mar. 2014.

[24] Z. Zhang and S. Cuk, "A high efficiency 500 W step-up Cuk converter," in *Proc. IEEE Power Electron. Motion Control, Conf.*, 2000, pp. 909–914.

[25] C. Cui, G. Liu, and K. Wang, "A novel drive method for high-speed brushless DC motor operating in a wide range," *IEEE Trans. Power Electron.*, vol. 30, no. 9, pp. 4998–5008, Sep. 2015.

[26] X. F. Zhang and Z. Y. Lu, "A new BLDC motor drives method based on BUCK converter for torque ripple reduction," in *Proc. IEEE Power Electron. Motion Control, Conf.*, 2006, pp. 1–4.

[27] N. Mutoh, M. Ogata, K. Gulez, and F. Harashima, "New methods to suppress EMI noises in motor drive systems," *IEEE Trans. Ind. Electron.*, vol. 49, no. 2, pp. 474–485, Apr. 2002.

[28] D. Cochrane, D. Chen, and D. Boroyevich, "Passive cancellation of common-mode noise in power electronic circuits," *IEEE Trans. Power Electron.*, vol. 18, no. 3, pp. 756–763, May 2003.

Wei Chen (M'12) was born in Shanxi, China, in 1977. He received the B.Sc., M.Sc., and Ph.D. degrees in electrical engineering from Tianjin University, Tianjin, China, in 2000, 2003, and 2006, respectively.

In 2006, he joined Tianjin University as a Lecturer, where he has been an Associate Professor in the School of Electrical Engineering and Automation since 2009. His research interests include modeling optimization of electrical machines and their drivers.

Yapeng Liu was born in Anhui, China, in 1991. He received the B.S. degree from Liaoning Technical University, Liaoning, China, in 2014.

He is currently working toward the M.S. degree in electrical engineering in the School of Electrical Engineering and Automation, Tianjin University, Tianjin, China. His research interests include electrical machines, motor drives and power electronics.

Xinmin Li was born in Hunan, China, in 1989. He received the B.S. degree from the University of Science and Technology Beijing, Beijing, China, in 2011.

He is currently working toward the Ph.D. degree in electrical engineering in the School of Electrical Engineering and Automation, Tianjin University, Tianjin, China. His research interests include electrical machines and motor drives, power electronics, and wind power technology.

Tingna Shi (M'13) was born in Zhejiang, China, in 1969. She received the B.S. and M.S. degrees from Zhejiang University, China, in 1991 and 1996, respectively, and the Ph.D. degree from Tianjin University, China, in 2009, all in electrical engineering.

She is currently a Professor in the School of Electrical Engineering and Automation, Tianjin University, Tianjin, China. Her current research interests include electrical machines and their control systems, power electronics, and electric drives.

Changliang Xia (M'08–SM'12) was born in Tianjin, China, in 1968. He received the B.S. degree from Tianjin University, Tianjin, China, in 1990, and the M. S. and Ph.D. degrees from Zhejiang University, China, in 1993 and 1995, respectively, all in electrical engineering.

He is currently a Professor in the School of Electrical Engineering and Automation, Tianjin University, and also in Tianjin Key Laboratory of Advanced Technology of Electrical Engineering and Energy, Tianjin Polytechnic University. In 2008, he became a "Yangtze Fund Scholar" Distinguished Professor and is currently supported by the National Science Fund for Distinguished Young Scholars. His research interests include electrical machines and their control systems, power electronics, and control of wind generators.